Alqalam Journal of Medical and Applied Sciences. 2025;8(3):1977-1986
https://doi.org/10.54361/ajmas.2583102

Original article

Effect of Hydrogen Peroxide on Passive Film Behavior of 304L Stainless Steel

Hesham Mraied*, Asma Sharfeddin

Department of Materials and Metallurgical Engineering, University of Tripoli, Tripoli, Libya
***Corresponding email**: h.mraied@uot.edu.ly*

Abstract
Different grades of austenitic stainless steels, such as 304L, 316L, and nickel-free high-nitrogen austenitic stainless steels, are used in biomedical applications due to their biocompatibility, adequate mechanical properties, and excellent corrosion resistance. The performance of these alloys can be altered due to the presence of reactive species like hydrogen peroxide, a byproduct of the inflammatory response in the human body. In this study, the corrosion behavior of 304L stainless steel was investigated in normal saline solution doped with 8 ml/L hydrogen peroxide to simulate inflammation. Cyclic polarization, electrochemical impedance spectroscopy, and Mott-Schottky analysis were used to study the corrosion resistance, passive film stability, and semiconducting properties of the alloy. It was found that the addition of hydrogen peroxide increased the corrosion rate and defect density of the passive film and allowed for the growth of a thicker, still unstable oxide layer. These findings revealed the important role of oxidative environments (inflammatory conditions) on the corrosion behaviour of 304L stainless steel. Thus, the significance of advanced alloy design, surface modifications, and protective measures to enhance corrosion resistance under such conditions is emphasized.
Keywords: Austenitic Stainless Steel, Hydrogen Peroxide, EIS, Cyclic Polarization

Introduction

Any material to be inserted into a human body needs to be biocompatible. If not, the material could lead to negative reactions such as inflammation, allergic responses, and toxicity. After being implanted, biomaterials must endure the mechanical stresses that could lead to failure. Additionally, biomaterials require exceptional resistance to corrosion and wear in physiological environments [1]. The composition of the physiological environment into which biomaterials are implanted varies from one location to another in the human body. In general, the environment contains different types of organic and inorganic species such as ions, amino acids, proteins, and living cells. The deterioration of the biomaterial, as well as inflammatory conditions, can alter the composition of the environment [2]. In physiological environments, the presence of microorganisms on the surface of metals could alter the concentration of the different species in the electrolyte, pH, and oxygen level, which may lead to localized corrosion [3]. The release of metallic ions in concentrations higher than those tolerable to human tissue, because of degradation of the implant, can cause metal allergy, carcinogenicity, cytotoxicity, and genotoxicity [4-6].

Hydrogen Peroxide (HP) is one of the reactive oxygen species (ROS) present in vivo and has been used to simulate inflammatory conditions. HP is produced by activated phagocytes and leukocytes and the subsequent formation of hydroxyl radicals, singlet oxygen, and additional HP. Moreover, the presence of HP plays an important role in the corrosion process of the alloy in biomedical applications by breaking down the passive layer, introducing defects, and, in turn, speeding up the materials' degradation. Therefore, it is critical to study these issues to design materials and solutions that can reduce corrosion in aggressive environments [7, 8].

Stainless steels, particularly the austenitic types like 304L stainless steel, are known for their excellent corrosion resistance and mechanical strength as well as suitability for applications in different industries. These properties are mainly the result of the formation of a passive chromium-rich oxide film that acts as a barrier against environmental attack. The low carbon content in 304L stainless steel decreases the precipitation of the carbides, which improves its resistance to intergranular corrosion. Although stainless steels have excellent corrosion resistance in most environments, the presence of very aggressive species such as chlorides and biofluids can lead to local attacks such as pitting and crevice corrosion [9]. Various methods have been explored to improve the corrosion resistance of stainless steel, mainly by reducing the number of nonmetallic inclusions, particularly chromium carbide. For instance, techniques such as vacuum arc re-melting as well as increasing the levels of chromium, molybdenum, and nitrogen have been shown to enhance passivity and resistance to localized corrosion. Additionally, other materials like Ti and Co-Cr-Mo were found to possess superior corrosion resistance in biological environments compared to austenitic stainless steels [1,10].

Ferrer et al. [11] studied the action of abrasion and corrosion on AISI 304L stainless steel in saline solution. They used acoustic emission and electrochemical methods, which showed that mechanical abrasion greatly speeds up the corrosion process. The acoustic emission method was able to detect and characterize the beginning and progress of corrosion under abrasive conditions. Soliz et al. [12] studied the erosion–corrosion of AISI 304L stainless steel in 0.5 M NaCl solution with the addition of industrial

***Copyright** Author (s) 2025. Distributed under Creative Commons CC-BY 4.0*
***Received**: 12-07-2025 - **Accepted**: 10-09-2025 - **Published**: 18-09-2025*

tailing particles from the copper mining industry. They looked at pure corrosion, pure erosion, and their synergetic effect on total wear rate using potentiodynamic and weight loss techniques. They reported that chemical reagents in the tailings greatly affect the corrosion rate and that pure erosion plays a greater role in total wear than pure corrosion. Modiri et al. [13] studied the corrosion behavior of 304L stainless steel coated with a thin layer of manganese-nitride (Mn-N) in a saline solution. It was found that the Mn-N coating does, in fact, improve the corrosion resistance of the stainless steel by enhancing passivation in the electrolyte. This treatment may be a good approach for the protection of stainless steel in high chloride environments. In a related study by Guidic et al. [14], who studied the corrosion of many types of stainless steels, including 304L in a phosphate-buffered saline (PBS) solution at pH 7.4, a typical environment representing biomedical applications. The study showed that alloy 304L exhibited moderate corrosion resistance, but it was prone to pitting corrosion due to the presence of chlorides. Salih et al. [15] investigated the effects of chloride and iodide ions on the pitting corrosion of 304 and 304L stainless steels. They reported that both alloys underwent pitting corrosion due to the presence of chlorides. Pitting corrosion was even worse as the temperature increased. The effect of iodide ions was less aggressive compared to that of chloride ions. In other work by Simionescu et al. [16], the role of HP and lactic acid present in bio-salvia in the corrosion resistance of 304L stainless steel was studied. It was found that the addition of HP increased the corrosion rate of the alloy due to the breakdown of the passive film.

The objective of this research is to investigate the role of HP on the passive film behaviour of 304L stainless steel in normal saline solution. Cyclic polarization (CP), Electrochemical Impedance Spectroscopy (EIS), and Mott-Schottky analysis (MS) were used to investigate the changes in corrosion resistance, passive film stability, and semiconducting properties of the alloy in this simulated biological environment with and without the addition of HP.

Experimental Procedure

Material Preparation and Characterization

The material used in this research was cut from a cylinder of 304L stainless steel. The chemical composition (in mass fractions, wt %) was 19.5 Cr, 10.5 Ni, 2.0 Mn, 0.10 N, 1.0 S, 0.03 C, 0.045 P, 0.015 S, and Fe (balance). For microstructural analysis and electrochemical tests, samples of area 3.8 cm^2 and 4 cm thickness were cut from the cylinder using Wire Electric Discharge Machine (WEDM), after which the samples were mounted in epoxy resin. Before the electrochemical tests, a copper wire was welded to one side of each sample. All samples were mechanically polished through a series of SiC papers up to 1200 grit, followed by polishing using 3 microns diamond paste to remove surface imperfections, and fine polishing with 0.5 microns alumina to obtain a mirror-like, scratches free surface. The microstructure was examined by electro etching a polished sample with a solution of 10 grams of oxalic acid in 100 ml of distilled water. The electro-etching was conducted at 6 volts with the sample as an anode to improve the visibility of grain boundaries and inclusions, thus enabling precise microstructure analysis.

Electrochemical Testing

The electrochemical measurements, including CP, EIS, and MS analysis, were conducted using a Gamry Reference 600® potentiostat in a naturally aerated and stagnant 0.9 wt.% NaCl (Normal saline) solution simulating body fluid environment. To simulate inflammatory conditions, the normal saline solution was doped with 8 mL / L of 30% concentration HP (Normal saline + HP). The selection of this concentration of HP in normal saline to model inflammation was intentionally chosen to induce a sub-lethal, yet potent, oxidative stress that recapitulates key biochemical features of the inflammatory response. This concentration (equivalent to approximately 7 mM HP) serves as an experimental proxy for the respiratory burst of innate immune cells, such as neutrophils and macrophages, which generate ROS including superoxide anion (O_2^-) and HP at sites of tissue injury or infection.

The electrochemical stability and alloy susceptibility to localized corrosion were examined using CP tests. The potential was swept from 0 V to 2 V versus Open Circuit Potential (OCP) at a forward scan rate of 0.5 mV/s and then reversed at the same scan rate to a final potential of 0 V versus OCP, thus completing the cyclic loop. The sample current density limit was set at an apex value of 10 mA/cm^2, and the sample period was 1 s. EIS tests were used to study the impedance behavior of the passive film. The frequency range was from 100 KHz to 0.01 Hz measured at 5 points per decade. A sine-wave AC voltage of 10 mVrms was applied with a DC voltage of 0 V versus OCP. The semiconducting behavior of the passive film was studied using MS analysis. The potential was swept between 0 V and -0.5 V vs OCP with a voltage amplitude of 10 mV_{rms}, sweep rate of 0.01 V, and frequency of 1 KHz. Electrochemical tests were carried out in a three-electrode electrochemical cell configuration. The sample, graphite rod, and a silver/silver chloride (Ag/AgCl) electrode were used as the working, counter, and reference electrode, respectively. Before measuring, the system was allowed to stabilize at the OCP for 60 min, and the preexisting surface ferric oxides/hydroxides were removed by conditioning the samples at -0.4 V vs. OCP for 3600 s. This will promote reproducible initial surface conditions. All electrochemical tests were conducted at room temperature. Electrochemical test data were obtained through the Gamry Framework software by linking the Gamry potentiostat to a computer. Data was then fitted and analyzed using Gamry E-chem Analyst

Copyright *Author (s) 2025. Distributed under Creative Commons CC-BY 4.0*
Received: *12-07-2025* - ***Accepted***: *10-09-2025* - ***Published***: *18-09-2025*

software. To ensure data reproducibility and accuracy, the results of at least three samples for each electrochemical test are reported.

Results And Discussion

Microstructure

The microstructure of 304L stainless steel is composed of an austenitic phase with face-centered cubic (FCC) grain structure. This structure provides the alloy with very good corrosion resistance, toughness, and formability. As shown in (Figure 1) the microstructure is composed of elongated or equiaxed grains, which depend on the processing history (for instance, rolling or annealing). The dark spots that appeared in the microstructure are most likely inclusions or precipitates such as manganese sulfides or chromium carbides [17]. The grain boundaries are distinct and may show the results of mechanical or thermal processing, like recrystallization or grain growth. When compared to standard 304, which has a higher carbon content, 304L stainless steel forms fewer chromium carbides and hence has a lower tendency to intergranular corrosion. Under specific thermal conditions, these faces may form at grain boundaries. Moreover, the reduced carbon content improves the weldability and resistance to sensitization, which in turn makes 304L stainless steel a suitable candidate in very corrosive environments like chemical processing and food production.

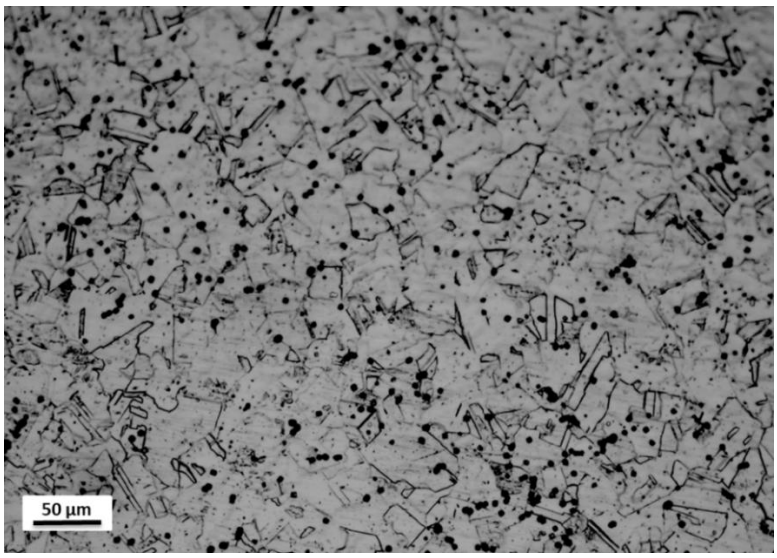

Figure 1. Microstructure of 304L stainless steel.

Electrochemical Tests

A typical CP curve of 304L stainless steel in normal saline and normal saline + HP solution is shown in (Figure 2). The scan direction is indicated by black arrows in the plots. The CP curves in both solutions exhibited a positive hysteresis, which normally occurs when the forward scan does not align with the reverse scan. This positive hysteresis indicates the continuous growth of pits. In this case, the backward scan has a slower decrease in current density. As a result, it is difficult to stop the propagation of these pits [18]. The extent of the hysteresis could be indicated by the difference in current density of the forward and reverse scan at the same potential. An increase in the hysteresis loop indicates larger disruption of a difficult-to-restore passive films [18].

The corrosion potential (E_{corr}) is the electrode potential where no external current is flowing through the system. It is a measure of the equilibrium between anodic (metal dissolution) and cathodic (reduction) reactions on the metal surface. In (Figure 2) a noble shift in E_{corr} was observed due to the addition of HP. This behavior may indicate the shift of the surface towards the cathodic (reduction) process or the metal is becoming less active (more resistant to corrosion) [19]. It is also important to note that this shift may not always indicate reduced corrosion, as it may result from the complex interplay of anodic and cathodic reactions [20]. On the other hand, the corrosion current density (i_{corr}) is indicative of the rate of metal dissolution (corrosion rate) and any increase in i_{corr} is a sign that the anodic reaction (metal dissolution) is in fact increasing [21].

Copyright *Author (s) 2025. Distributed under Creative Commons CC-BY 4.0*
Received*: 12-07-2025 -* ***Accepted****: 10-09-2025 -* ***Published****: 18-09-2025*

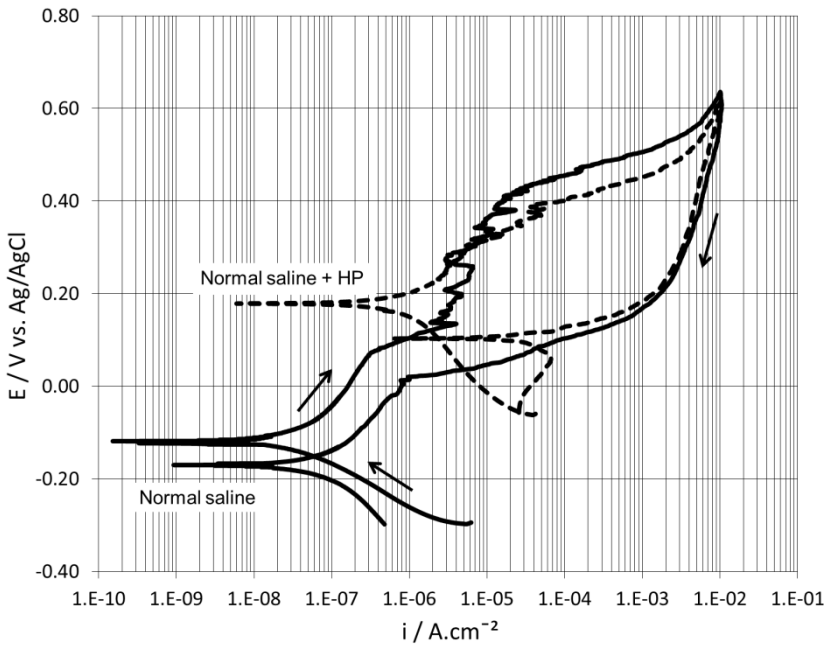

Figure 2. Typical CP scan of 304L stainless steel in normal saline solution and normal saline + HP solution.

The simultaneous increase in both E_{corr} and i_{corr} may either indicate the growth of the passive film or changes in the cathodic process (for example, oxygen reduction may have become more favorable). However, if the passive film becomes unstable or undergoes breakdown, an increase in the i_{corr} is expected due to greater metal dissolution. On the other hand, an increase in E_{corr} may result from an increase in the rate of the cathodic reactions, which in turn may cause an increase in i_{corr} if at the same time the anodic reaction (metal dissolution) speeds up to balance out the system. These scenarios are expected due to the coexistence of oxygen (8 ml / L HP) and chloride ions (0.9 wt.% NaCl), where oxygen may enhance the cathodic reactions while chlorides may cause passive film breakdown (increasing metal dissolution).
As shown in (Figure 2), in both solutions, E_{corr} is more positive than the anodic to cathodic transition potential, indicating that the material is in a stable passive state at E_{corr}. At higher anodic potentials, the alloy experienced irreversible changes, which include passive film breakdown or localized corrosion. Moreover, during the reverse scan, the delayed repassivation causes the transition from anodic to cathodic behavior to shift to a less noble potential. This behavior depends on the surface chemistry, adsorption processes, localized corrosion, and the kinetics of repassivation. The difference between these potentials is a good indicator of the alloy's corrosion resistance in its passive state, despite being prone to localized damage at higher anodic potentials [22].
The pitting potential (E_{pit}) of 304L stainless steel in normal saline and normal saline + HP solutions is 130 ± 15 mV vs. Ag/AgCl and 310 ± 20 mV vs. Ag/AgCl, respectively. It was documented elsewhere that the introduction of HP can significantly influence the E_{pit} of stainless steels. It was found that HP can act as an oxidizing agent that increases the E_{corr} while decreasing the E_{pit} [23], thus enhancing the susceptibility of the alloy to pitting corrosion. T. Shibata [24] found that passivation treatment of stainless steels using oxidizing agents such as HP and O_3 plays an important role in the development of a more stable passive film. This treatment may increase the E_{pit} and therefore improve the resistance to pitting corrosion by promoting the rapid formation of a stable and uniform passive film. Both HP and O_3 are strong oxidizers that increase the oxidation rate of chromium in the steel surface, leading to the enrichment of chromium oxide (Cr_2O_3) in the passive layer. This chromium-rich oxide film acts as a protective barrier, reducing the presence of free iron and minimizing localized corrosion sites. The total effect of HP on E_{pit} is very complex and is a function of different variables such as the concentrations of the HP and chloride ions present, pH levels, and the type of alloy.
The corrosion rate in µm/year shown in (Figure 3) was estimated by Faradic conversion of the i_{corr} (i.e., 1 µA/cm^2 corresponds to approximately 10 µm/year), supposing uniform corrosion of the metal (M) with the formation of M^{2+}. It was found that the corrosion rate of 304L stainless steel (0.11 ± 0.006 µm/year) in normal saline solution was increased to (0.98 ± 0.13 µm/year) due to the presence of HP in the electrolyte. This increase in corrosion rate is related to the increase in i_{corr} as discussed earlier.

Copyright *Author (s) 2025. Distributed under Creative Commons CC-BY 4.0*
Received: *12-07-2025* - ***Accepted***: *10-09-2025* - ***Published***: *18-09-2025*

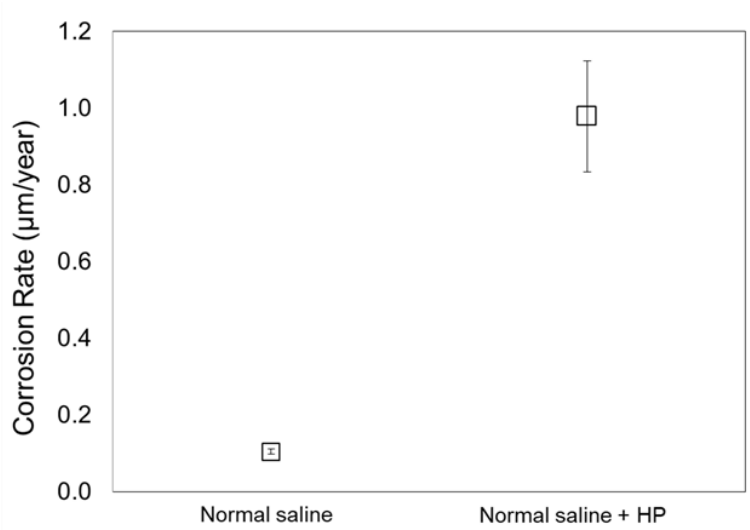

Figure 3: Corrosion rate of 304L stainless steel in normal saline solution and normal saline + HP solution obtained from the CP test.

To evaluate the electrochemical kinetics at the sample-electrolyte interface, EIS measurements were conducted in normal saline and normal saline + HP solution. The Nyquist diagram for representative results is shown in (Figure 4). The plots in the diagram were generally similar in having a single capacitive loop shape, indicating the formation of a protective passive film on the metal surface. This shape can also be expected from a polarization resistance due to Faradaic processes coupled with an interfacial charge storage process. When compared with that of the bare saline solution, the capacitive semicircle of the Nyquist plot becomes smaller with the presence of HP, indicating the reduction of the corrosion resistance in agreement with the results of the CP tests.

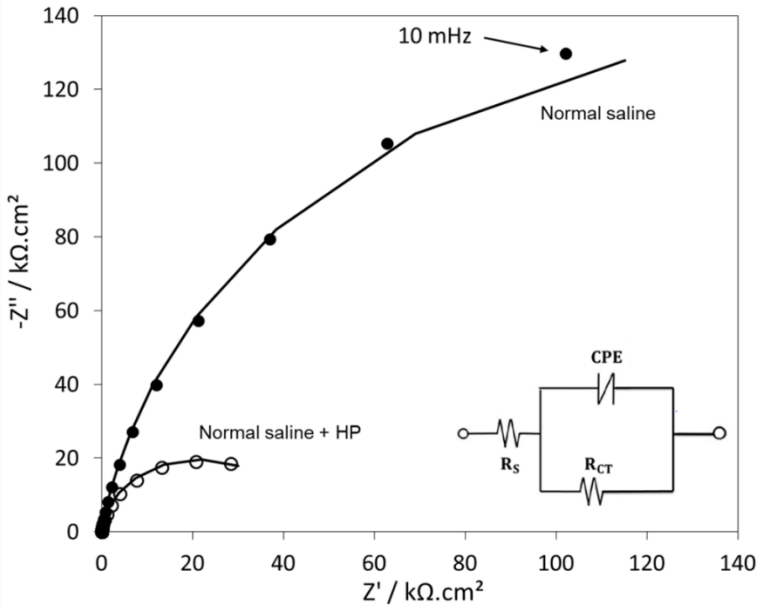

Figure 4: Representative Nyquist plots (scattered data) of 304L stainless steel in normal saline solution and normal saline solution + HP

The experimental data were interpreted using the analog equivalent circuit model shown as an inset in (Figure 4). This simplified Randles cell includes a solution resistance (Rs), a double-layer capacitor in the form of a constant phase element (CPE) in parallel with the charge transfer resistance (R_{CT}). The CPE was used taking into consideration the non-ideal capacitance behavior resulting from surface heterogeneity or disturbed time constant of charge transfer reactions [25].
The impedance of the non-ideal capacitance CPE is represented as (Equation 1):

$$Z_{CPE} = Y_o^{-1}(j\omega)^{-n}, \qquad (1)$$

Where Yo is a constant representing a base admittance, $j = (-1)^{1/2}$, ω is the angular frequency, and (n) is a frequency dependence exponent which measures the deviation from ideal capacitor behavior. The values of (n) are between 0 and 1. The CPE reduces to a simple capacitor with $C=Y_O$ when (n) =1. The numeric value

Copyright *Author (s) 2025. Distributed under Creative Commons CC-BY 4.0*
Received*: 12-07-2025 -* ***Accepted****: 10-09-2025 -* ***Published****: 18-09-2025*

of Y_O is roughly indicative of an effective interfacial capacitance, disregarding dimensional issues. As shown in (Figure 4), the fitted results (solid lines) closely matched the experimental behavior for almost all of the frequency range for all results.

The Rs of both electrolytes was in the range of 15 ± 4 Ω.cm^2. As expected, the values are consistent with the cell dimensions and electrolyte resistivity and independent of the material tested and electrolyte type. It should be noted here that when the R_{CT} is much larger than the Rs, the latter will not appear in Nyquist plots.

(Figure 5) shows the values of the parameters of the CPE elements (n and Y_O) obtained from fitting EIS data with the equivalent circuit shown in (Figure 4). As shown in (Figure 5.a), the values of (n) increased due to the addition of HP to the normal saline solution. The value of (n) indicates the capacitive behavior defined by the surface inhomogeneity of the steel at the interface with the electrolyte.

In the study by Luo et al. [26], the electrochemical behavior of 2205 duplex stainless steel in NaCl solution with varying chromate contents was investigated, highlighting the role of passive film properties in corrosion resistance. The addition of chromates enhanced passivation by stabilizing the oxide layer and suppressing pit initiation. As the number of pits decreased, the passive film surface became more uniform and continuous, reducing localized defects that normally act as conductive pathways for aggressive ion penetration. This smoother and less conductive film improved the capacitive nature of the metal/solution interface, which is associated with better charge storage and barrier properties. Consequently, the constant phase element exponent (n), which reflects the degree of ideal capacitive behavior, increased, indicating a stronger capacitive interface and a more protective passive layer

As shown in (Figure 5,b). The values of Y_O decreased due to the addition of HP to the normal saline solution. A decrease in the Y_O can be related to the increase in the thickness of the passive film formed on the surface of the sample [27].

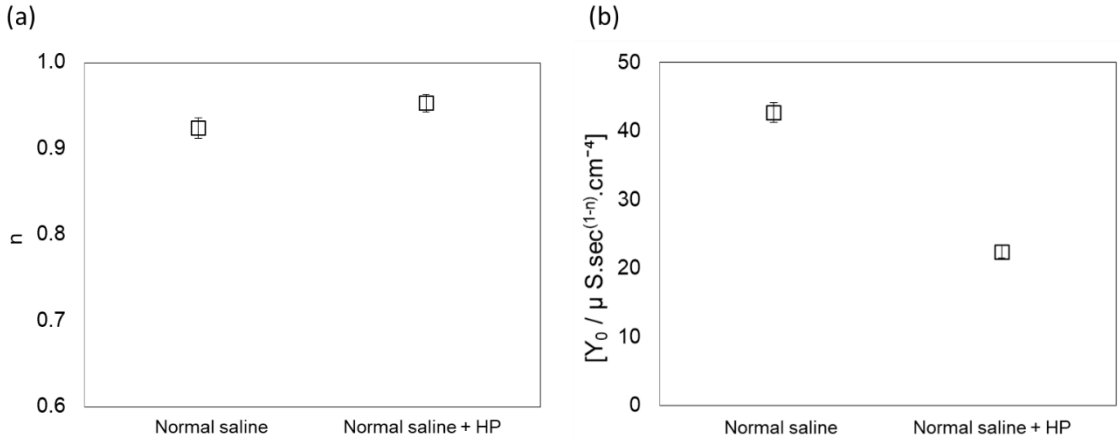

Figure 5: Magnitudes derived from EIS tests (a) n, (b) Yo of 304L stainless steel after immersion in normal saline and normal saline + HP solution. The error bars represent the standard deviation of the data.

As (n) approaches the value of 1, the CPE parameter Y_O may be viewed as a rough estimate of the film capacitance C as per (Equation 2):

$$C = Y_o.sec^{n-1}, \quad (2)$$

In our previous work [28], the corrosion resistance of Al and Al–Mn thin films was analyzed using EIS, where the constant phase element CPE is often used to represent non-ideal capacitive behavior. It was emphasized that the accuracy of interpreting EIS data strongly depends on the value of the exponent (n). When (n) = 1, the CPE behaves as an ideal capacitor, accurately reflecting the capacitive response of a uniform passive film. However, as (n) decreases from unity, the system deviates from ideal capacitive behavior due to surface inhomogeneities, roughness, or localized corrosion defects. Under such conditions, the mathematical expression used to model the impedance becomes increasingly inaccurate, limiting its reliability for describing the electrochemical interface. A nominal thickness of the passive film (d) may be obtained from (Equation 3):

$$d = \varepsilon\varepsilon_o A/C, \quad (3)$$

where ε is the dielectric constant of the passive film (taking it to be ~15.6 for stainless steel, ε_o is the permittivity of vacuum (8.85 x 10^{-14} F.cm^{-1}), and A is the exposed surface area (~3.8 cm^2). (Equation 3) supports the finding shown in (Figure 5). Since C (or Y_O) is inversely proportional to the thickness of the protective layer (d), the decrease in the capacitance by the addition of HP increased the thickness of the protective layer.

Copyright *Author (s) 2025. Distributed under Creative Commons CC-BY 4.0*
Received*: 12-07-2025 -* ***Accepted****: 10-09-2025 -* ***Published****: 18-09-2025*

The passive film thickness of 304L stainless steel when exposed to normal saline solution was (2.23 ± 0.12 nm). These values are comparable to those reported in other investigations for oxide films formed on the steel surface in different media [26, 29], thus supportive of the interpretation of the constant phase element parameters represented in (Equations 1 through 3). The thickness of the passive film increased to (5.34 ± 0.24 nm) when normal saline was doped with HP.

The decomposition of HP to water in aerated media, as shown in (Equations 4 and 5), can catalyze the formation of metal oxide by enhancing the oxygen reduction reaction (Equation 6). This would result in the growth of the oxide film.

$$2H_2O_2 \rightarrow O_2 + 2H_2O \quad (4)$$

$$H_2O_2+2H^++2e^- \rightarrow 2H_2O \quad (5)$$

$$O_2+4H^++4e^- \rightarrow 2H_2O \quad (6)$$

The R_{CT} of 304L stainless steel was decreased from ~440 ± 20 kΩ.cm^2, when exposed to normal saline to 44 ± 3 kΩ.cm^2 when normal saline was doped with HP. This reduction in R_{CT} may enhance the ionic conductivity and increase the electrochemical activity of the alloy at the interface with the electrolyte. HP may break down into reactive oxygen species and other intermediates, which in turn facilitate electron and ion transport. These reactive species interact with the electrolyte's ionic components to create paths for charge transfer, which in turn lowers the energy for electron flow. As a result, the R_{CT} decreases [30].

The corrosion current density (i_{corr}) from EIS tests was estimated from the R_{CT} using the Stern-Geary Equation: [31, 32]:-

$$i_{corr} = B/R_{CT}, \quad (7)$$

where B is the apparent Stern-Geary coefficient, which can be estimated from [31, 32]:

$$B = \frac{\beta_a.\beta_c}{2.3(\beta_a + \beta_c)} \quad (8)$$

where β_a and β_c are the anodic and cathodic Tafel slopes, respectively, measured from cyclic potentiodynamic polarization experiments. The validity of corrosion current densities estimated from the Stern-Geary equation depends on the correct determination of the coefficient B and whether a metal (M) dissolves directly to M^{2+} or through an M^+ intermediate [32-34].

In this work, the value of B was chosen to be equal to 0.052 V, a value that is commonly used for systems where the anodic and cathodic reactions are under activation control and Tafel slopes are within a normal range. i_{corr} was converted to corrosion rate (C.R) in micrometers per year as shown in (Figure 6) using Faraday's conversion (1 µA.cm^{-2} ≈ 10 µm/y), a typical value measured for many engineering materials, assuming uniform corrosion for the different components of the alloy [35].

As shown in (Figure 6), the nominal corrosion rate of 304L stainless steel estimated from EIS decreased because of the addition of HP to normal saline solution. This decrease is related to the decrease in R_{CT} discussed earlier and is compatible with the values obtained from the CP test.

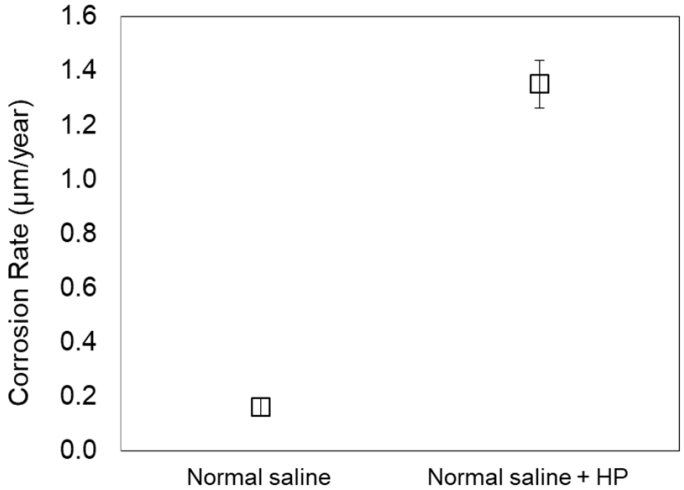

Figure 6: Corrosion rate of 304L stainless steel in normal saline solution and normal saline + HP solution obtained from EIS test.

MS experiments were conducted in the cathodic potential range to study the electronic properties of the passive film. This range was selected to avoid the dissolution or breakdown of the passive film that may occur at anodic potentials, which is a common issue in aggressive environments such as those rich with chlorides. Moreover, in the cathodic region, it is expected to experience minimal redox reactions, allowing for accurate measurement of capacitance and the determination of donor/acceptor density without the interference of faradaic currents. The passive film stability is key in studying the semiconducting properties of the passive film. At cathodic potentials, passive film thinning or localized pitting is not expected, which can keep the passive film in good condition during the experiment. Other studies have reported that the use of cathodic MS analysis gives out reliable results and valuable insight into the

Copyright *Author (s) 2025. Distributed under Creative Commons CC-BY 4.0*
Received*: 12-07-2025 -* ***Accepted****: 10-09-2025 -* ***Published****: 18-09-2025*

electronic structure and defect density of passive films on stainless steel, helping in a better understanding of their corrosion resistance mechanisms [35].

The MS of 304L stainless steel in normal saline and normal saline + HP solution (Figure 7) revealed the semiconducting performance of the passive film. In both solutions, the passive film displays n-type semi conducting behavior (eq. 9). The n-type semiconductors are characterized with acceptor dominance (e.g., ion vacancies or oxygen interstitials), which play the primary role in conduction.

$$\frac{1}{C^2} = \frac{-2}{\varepsilon\varepsilon_0 e N_a}\left(E - E_{fb} - \frac{KT}{e}\right) \quad (9)$$

where C is the capacitance, ε is the dielectric constant of the passive film (15.6 for AISI 304L stainless steel [36]), ε_o is the permittivity of vacuum (8.85×10^{-14} Fcm^{-1}), N_a is the acceptor density, E is the applied potential, E_{fb} is the flat band potential, K is Boltzmann constant (1.38×10^{-23} JK^{-1}), T is the absolute temperature, and e is the elementary charge (1.602×10^{-19} C).

As shown in (Figure 7), in normal saline solution, MS curves exhibited two separate linear trends with different slopes. This change in slope may be related to the change in the semiconducting properties of the layer-structured oxide film. In the case of normal saline + HP solution (shown as an inset in (Figure 7) for clarity), a shift towards more positive potentials along with flatter slopes in both regions was observed. This behavior may be related to the higher carrier density and defect concentration within the passive film because of the oxidizing nature of HP. The introduction of HP may also cause the formation of defects such as oxygen interstitials, or may change the oxide composition, which may increase the conductivity of the passive film, as well as reducing its stability. The change in the flat band potential due to the addition of HP may indicate that the chemical and electronic properties of the oxide layer are greatly changed. These changes imply that the passive film becomes less protective and more susceptible to localized corrosion processes, such as pitting.

`The acceptor density shown in (Figure 8) was calculated using Equation 9. The acceptor density of the passive film of 304L stainless steel immersed in normal saline solution and normal saline solution + HP was $2.86 \times 10^{19} \pm 1.71 \times 10^{19}$ /cm^3 and $2.73 \times 10^{20} \pm 6.47 \times 10^{19}$ /cm^3, respectively.

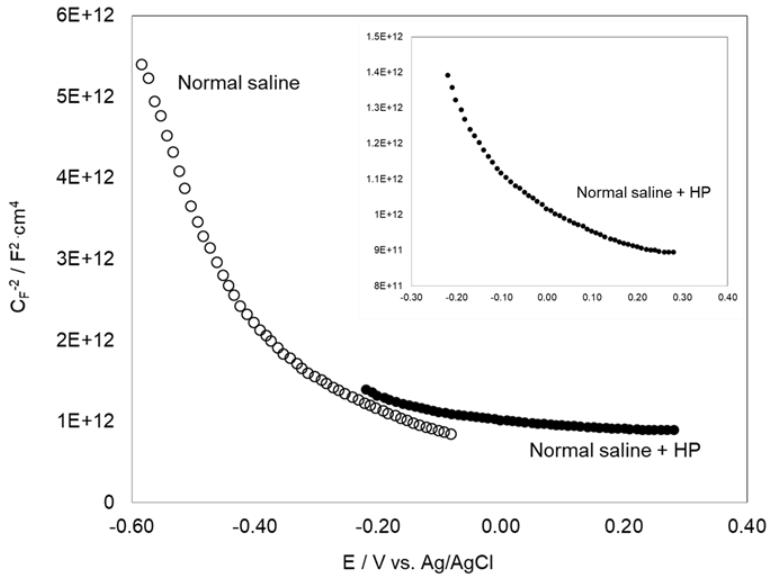

Figure 7: MS plots of passive films formed on 304L stainless steel after immersion in normal saline and normal saline + HP solutions

It should be noted here that the results from MS analysis are in good agreement with what was obtained from both CP and EIS experiments of the same samples in each solution. In general, in saline + HP solution, there was an increase in acceptor density and a drop in passivity, which was noted through flattening of MS curves and the shifted flat band potential. These findings could be related to the increase in localized corrosion attack noted in CP experiments. Moreover, the increase in defect density noted from the MS analysis is compatible with the decrease in impedance in EIS experiments. These complementary results suggest that HP greatly changes the electrochemical behavior, thus reducing the protective properties of the oxide film of 304L stainless steel, leading to enhanced corrosion susceptibility.

Copyright *Author (s) 2025. Distributed under Creative Commons CC-BY 4.0*
Received*: 12-07-2025 -* ***Accepted****: 10-09-2025 -* ***Published****: 18-09-2025*

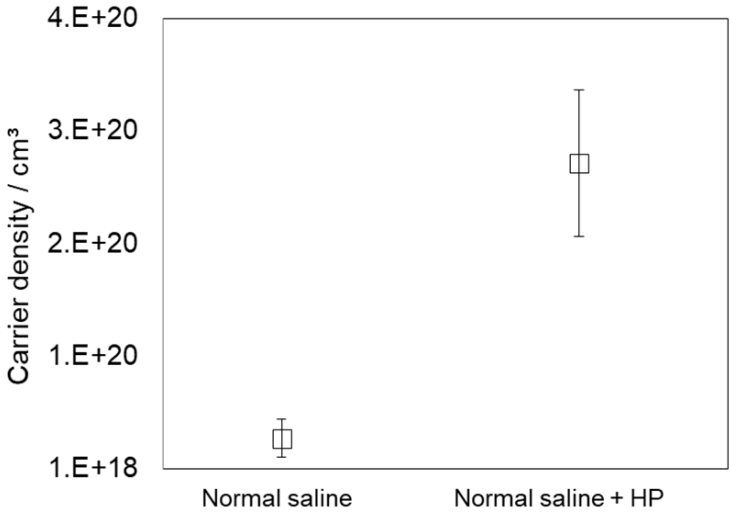

Figure 8: Carrier density of passive films formed on 304L stainless steel after immersion in normal saline and normal saline + HP solutions

Conclusions

The presence of HP greatly increases the corrosion rate of 304L stainless steel in saline solutions, indicated by the increase in corrosion current density and reduction in charge transfer resistance. HP changes the passive properties of the protective oxide film, indicated by higher defect density, increased conductivity, and reduced stability of the film, making the material more prone to localized corrosion. The passive film formed in the presence of HP was characterized by a higher acceptor density and defect concentrations as determined by MS analysis, indicating a less protective oxide layer. The addition of HP promotes the growth of a thicker passive film due to enhanced oxidation processes, while increased defect density, which plays a role in the loss of the film's corrosion resistance. CP tests showed that in the presence of HP, there is a large increase in hysteresis, indicating a greater difficulty in repassivating pits once they have formed. Finally, the results of EIS, CP, and MS all suggested that in chloride-containing environments, HP negatively influences the corrosion resistance of 304L stainless steel.

Funding

This research received no external funding.

Conflicts of Interest

The authors declare no conflicts of interest.

References

1. Manivasagam G, Dhinasekaran D, Rajamanickam A. Biomedical implants: corrosion and its prevention - a review. Recent Patents Corros Sci. 2010;2:40–54.
2. Dragus L, et al. Effect of the inflammatory conditions and albumin presence on the corrosion behavior of grade 5 Titanium alloy in saliva biological solution. IOP Conf Ser Mater Sci Eng. 2019;572(1):012005.
3. Xu C, et al. Corrosion and electrochemical behavior of 316L stainless steel in sulfate-reducing and iron-oxidizing bacteria solutions. Chin J Chem Eng. 2006;14:829–34.
4. Lü X, et al. Mechanisms of cytotoxicity of nickel ions based on gene expression profiles. Biomaterials. 2009;30(2):141–8.
5. Zhang F, et al. Screening and validation of nickel ion cytotoxicity biomarkers based on transcriptomic and proteomic technology. Regen Biomater. 2022;9:rbac073.
6. Saulis G, Rodaitė-Riševičienė R, Saulė R. Cytotoxicity of a cell culture medium treated with a high-voltage pulse using stainless steel electrodes and the role of iron ions. Membranes (Basel). 2022;12(2).
7. Aslan C, Gilbert JL. In vitro corrosion assessment of the Essure® medical device in saline, simulated inflammatory solution and neutral buffered formalin. Acta Biomater. 2022;147:414–26.
8. Radice S, et al. Nickel-free high-nitrogen austenitic steel outperforms CoCrMo alloy regarding tribocorrosion in simulated inflammatory synovial fluids. J Orthop Res. 2022;40(6):1397–408.
9. Radice S, et al. Corrosion resistance of the nickel-free high-nitrogen steel FeCrMnMoN0.9 under simulated inflammatory conditions. J Biomed Mater Res B Appl Biomater. 2021;109(6):902–10.
10. Gurappa I. Characterization of different materials for corrosion resistance under simulated body fluid conditions. Mater Charact. 2002;49(1):73–9.
11. Ferrer F, et al. A study of abrasion–corrosion of AISI 304L austenitic stainless steel in saline solution using acoustic emission technique. NDT E Int. 2000;33(6):363–71.
12. Soliz Á, et al. Erosion–corrosion of AISI 304L stainless steel affected by industrial copper tailings. Metals. 2020;10(8):1005.

Copyright *Author (s) 2025. Distributed under Creative Commons CC-BY 4.0*
Received*: 12-07-2025 -* ***Accepted****: 10-09-2025 -* ***Published****: 18-09-2025*

13. Modiri F, Savaloni H. A study of the corrosion of stainless steel 304L coated with a 190 nm-thick manganese layer and annealed with nitrogen flux in a 0.4-mole solution of H2SO4 at different temperatures. J Theor Appl Phys. 2020;14(1):21–35.
14. Gudić S, et al. Corrosion behavior of different types of stainless steel in PBS solution. Sustainability. 2022;14(14):8935.
15. Salih SM, Shakir IK, Al-Sammarraie AM. Comparison of aggressiveness behavior of chloride and iodide solutions on 304 and 304L stainless steel alloys. Mater Sci Appl. 2017;8(12):889.
16. Simionescu N, Benea L, Chiriac A. The effect of H2O2 and lactic acid addition in biological saliva on the corrosion behaviour of 304L stainless steel. In: IOP Conf Ser Mater Sci Eng. 2020. IOP Publishing.
17. Hu C, et al. Investigation on microstructure and properties of the local dry underwater TIG welding of 304L stainless steel. Mater Today Commun. 2025;44:111978.
18. Esmailzadeh S, Aliofkhazraei M, Sarlak H. Interpretation of cyclic potentiodynamic polarization test results for study of corrosion behavior of metals: a review. Prot Met Phys Chem Surfaces. 2018;54:976–89.
19. Little BJ, Wagner PA, Lewandowski Z. Spatial relationships between bacteria and mineral surfaces. Rev Mineral. 1997;35:123–60.
20. Kolotyrkin YM, Losev V, Chemodanov A. Relationship between corrosion processes and oxygen evolution on anodes made from noble metals and related metal oxide anodes. Mater Chem Phys. 1988;19(1–2):1–95.
21. Wang S, et al. Relationship between dissolved oxygen and corrosion characterization of X80 steel in acidic soil simulated solution. Int J Electrochem Sci. 2015;10(5):4393–404.
22. Machado JEO. Oxide film development on a titanium alloy surface exposed to a physiological solution. University of Illinois at Chicago; 2021.
23. Makjan S, et al. Effects of hydrogen peroxide on 304 stainless steel in high temperature water. J Phys Conf Ser. 2019;1380(1):012087.
24. Shibata T. Increase in corrosion resistance of stainless steels by passivation treatment using (H2O2+O3) solution. Zairyo-to-Kankyo. 2010;59:464–7.
25. Alexander C, Tribollet B, Orazem M. Contribution of surface distributions to constant-phase-element (CPE) behavior: 1. Influence of roughness. Electrochim Acta. 2015;173.
26. Luo H, et al. Electrochemical behavior of 2205 duplex stainless steel in NaCl solution with different chromate contents. J Mater Eng Perform. 2012;21(7):1283–91.
27. Ghanem W, et al. Effect of nitrogen on the corrosion behavior of austenitic stainless steel in chloride solutions. Mod Appl Sci. 2015;9:119.
28. Mraied H, Cai W, Sagüés AA. Corrosion resistance of Al and Al–Mn thin films. Thin Solid Films. 2016;615:391–401.
29. Gudić S, et al. Corrosion behavior of different types of stainless steel in PBS solution. Sustainability. 2022;14:8935.
30. Bard AJ, Faulkner LR. Electrochemical methods: fundamentals and applications. Surf Technol. 1983;20(1):91–2.
31. King AD, Birbilis N, Scully JR. Accurate electrochemical measurement of magnesium corrosion rates; a combined impedance, mass-loss and hydrogen collection study. Electrochim Acta. 2014;121:394–406.
32. Bland LG, et al. Assessing the corrosion of commercially pure magnesium and commercial AZ31B by electrochemical impedance, mass-loss, hydrogen collection, and inductively coupled plasma optical emission spectrometry solution analysis. Corrosion. 2015;71(2):128–45.
33. Pardo A, et al. Electrochemical estimation of the corrosion rate of magnesium/aluminium alloys. Int J Corros. 2010;2010.
34. Petty RL, Davidson AW, Kleinberg J. The anodic oxidation of magnesium metal: evidence for the existence of unipositive magnesium. J Am Chem Soc. 1954;76(2):363–6.
35. Liu D, et al. A comparative study of the corrosion stability of dental amalgams with electrochemical impedance measurements. Mater Corros. 2020;71(6):949–55.
36. González JA, et al. Characterization of porous aluminium oxide films from a.c. impedance measurements. J Appl Electrochem. 1999;29(2):229–38.

Copyright *Author (s) 2025. Distributed under Creative Commons CC-BY 4.0*
Received*: 12-07-2025 -* ***Accepted****: 10-09-2025 -* ***Published****: 18-09-2025*